Rapid Communication

A novel method of rapidly modeling optical properties of actual photonic crystal fibres*

Wang Li-Wen(王立文), Lou Shu-Qin(娄淑琴)†,
Chen Wei-Guo(陈卫国), and Li Hong-Lei(李宏雷)

Key Lab of All Optical Network & Advanced Telecommunication Network of EMC, Beijing Jiaotong University, Beijing 100044, *China*
Institute of Lightwave Technology, Beijing Jiaotong University, Beijing 100044, *China*

(Received 8 March 2010; revised manuscript received 6 April 2010)

The flexible structure of photonic crystal fibre not only offers novel optical properties but also brings some difficulties in keeping the fibre structure in the fabrication process which inevitably cause the optical properties of the resulting fibre to deviate from the designed properties. Therefore, a method of evaluating the optical properties of the actual fibre is necessary for the purpose of application. Up to now, the methods employed to measure the properties of the actual photonic crystal fibre often require long fibre samples or complex expensive equipments. To our knowledge, there are few studies of modeling an actual photonic crystal fibre and evaluating its properties rapidly. In this paper, a novel method, based on the combination model of digital image processing and the finite element method, is proposed to rapidly model the optical properties of the actual photonic crystal fibre. Two kinds of photonic crystal fibres made by Crystal Fiber A/S are modeled. It is confirmed from numerical results that the proposed method is simple, rapid and accurate for evaluating the optical properties of the actual photonic crystal fibre without requiring complex equipment.

Keywords: photonic crystal fibre, digital image processing, finite element method, modeling optical properties

PACC: 4281, 4281C

1. Introduction

Photonic crystal fibres (PCFs) were demonstrated first in 1996,[1] and since then they have attracted considerable attention due to their flexible structures and novel optical properties, which empower the fibres to have enormous potential applications in diverse fields.[2−4] However, the flexible structure also brings some challenges to the fabrication of PCF. It is difficult to keep the position, the size and the shape of air holes during their fabrication. This would cause the resulting geometry of the actual fibre to inevitably deviate from the designed structure. Therefore, the optical properties of the resulting fibre would be different from the expected properties of the designed structure, which are negative for the application of photonic crystal fibre. So it is important to understand the optical properties of the actual fibre for the practical applications.

Up to now, some methods have been employed to measure the properties of the actual PCF such as pulse delay, phase-shift, super-continuum pulses or interferometer methods for the dispersion,[5−7] the scanning wavelength method,[8−11] Jones matrix eigen-analysis[12,13] or magneto-optic method[14] for the birefringence,[15,16] and the method reported in Ref. [17] for the mode cutoff phenomena. However, those methods often require a long fibre sample or complex expensive equipments. To our knowledge, there are few studies of modeling an actual photonic crystal fibre and evaluating its properties rapidly for the purpose of application. In this paper, a novel method, based on the combination model of digital image processing and finite element method, is proposed to rapidly model the optical properties of the actual PCF. With the proposed method, two kinds of photonic crystal fibres made by Crystal Fiber A/S are modeled.

*Project supported by the National Basic Research Program of China (Grant No. 2010CB328206), the National Natural Science Foundation of China (Grant No. 60977033) and the Science and Technology Innovation Foundation for Excellent Doctors of Beijing Jiaotong University, China (Grant Nos. 141055522 and 141060522).
†Corresponding author. E-mail: shqlou@bjtu.edu.cn
© 2010 Chinese Physical Society and IOP Publishing Ltd

2. Description of the novel method

In order to model the optical properties of the actual PCF, the novel method combines digital image processing technique with finite element method together to analyse the PCF. The flow chart is shown in Fig. 1. The first step is to obtain the cross-sectional image of the actual PCF, which can be completely achieved by the digital microscope. The following step is to rebuild the geometry structure of the cross section of the actual PCF by a series of digital signal processing technique including image magnification, threshold calculation, binary processing, noise elimination, edge extraction, geometry formation, and coordinate system transformation. Finally, finite-element method[18,19] is used for the modal solver in the actual PCF. Here, we concentrate on how to use the digital image processing technique to rebuild the cross-sectional structure of the actual PCF.

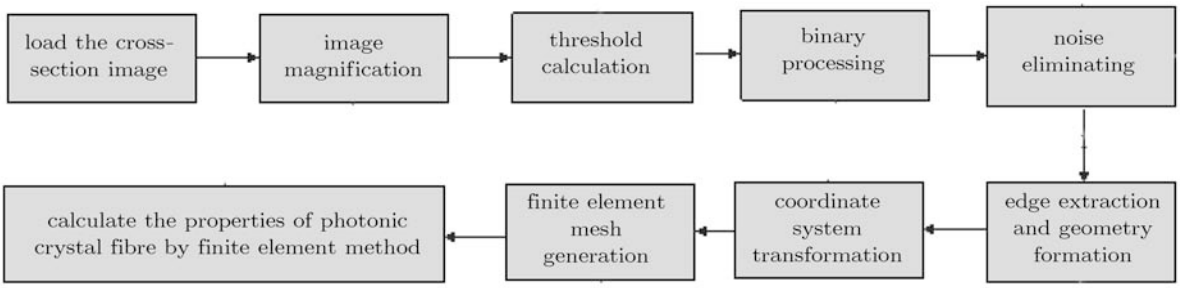


Fig. 1. Flow chart of the proposed novel method.

2.1. Rebuilding cross section of actual PCF by digital signal processing technique

The cross section of an actual PCF made by ourselves, which has been collected by digital microscope, is shown in Fig. 2. In order to improve image recognition accuracy, the original image needs to be magnified first. The enlarged image which is two times as big as the original one is also shown in Fig. 2. Cubic convolution interpolations[20,21] is employed to magnify the original image and the theory of this magnification method is described in Fig. 3.

Assuming that f is a sampled function and g is the corresponding interpolation function, then $g(x_k) = f(x_k)$ where x_k is an interpolation node. For equally spaced data as shown in Fig. 3(a), the interpolation function can be written as[21,22]

$$g(x) = \sum_k c_k u\left(\frac{x - x_k}{h}\right), \tag{1}$$

where h represents the sampling increment such as $h = x_1 - x_0$, x_k is a set of the interpolation nodes, u is the interpolation kernel, g is the interpolation function, c_k is a series of parameters which depend on the sampled data to make sure that the interpolation condition $g(x_k) = f(x_k)$ for each x_k to be satisfied. Then the kernel of cubic convolution interpolation is built up by a third-order polynomial and is given as

$$u(s) = \begin{cases} \frac{3}{2}|s|^3 - \frac{5}{2}|s|^2 + 1, & 0 < |s| < 1, \\ -\frac{1}{2}|s|^3 + \frac{5}{2}|s|^2 - 4|s| + 2, & 1 < |s| < 2, \\ 0, & 2 < |s|, \end{cases} \tag{2}$$

where s is defined as $s = (x - x_0)/h$.

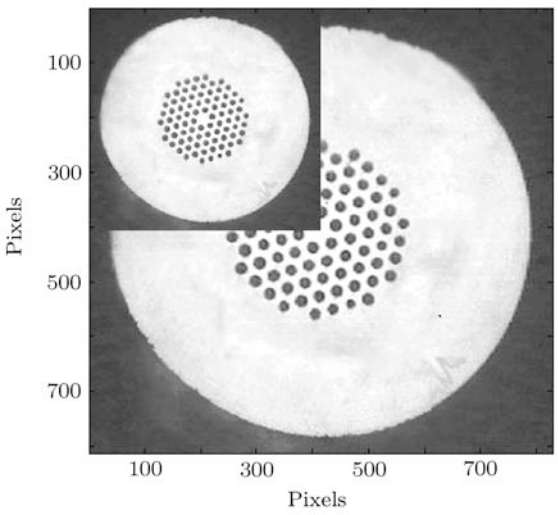


Fig. 2. Comparison between the original image and the enlarged cross-sectional image.

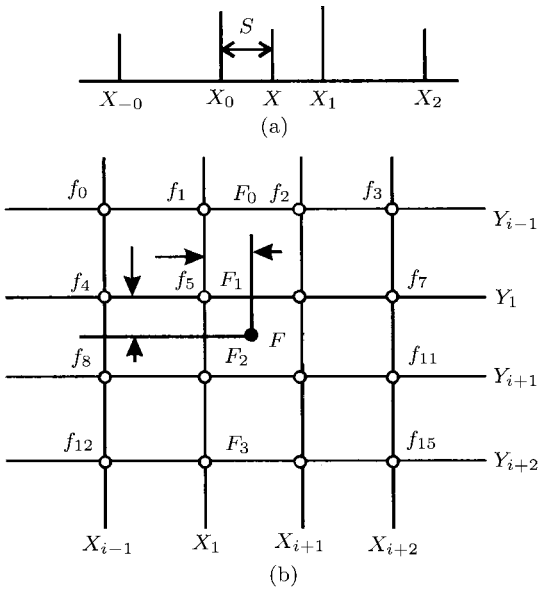


Fig. 3. Schematic diagram of convolution interpolation principle.

In order to obtain the pixel value of the interpolation point F as shown in Fig. 3(b), the pixel value of four temporary interpolation points (F_0, F_1, F_2, F_3) of every row should be calculated first by the cubic interpolation method and then the pixel value of point F could be obtained by the four temporary points of the column. With this method, the original image in Fig. 2 is enlarged two times, which is shown in Fig. 2 as well. The small one in Fig. 2 is the original image whose size is 406×414 in pixel and the larger one in Fig. 2 is the enlarged image whose size is 812×828 in pixel.

After the image magnification, the most important step is to calculate the threshold and perform the binary processing which converts a grayscale or colourful image into a binary image with only two colours: black (0) and white (1). The advantage of binary image is easy for us to eliminate noise and extract the boundary of neighbourhoods. The threshold is crucial for determining whether the extracted geometry of PCF will accurately represent the cross session of actual PCF. Based on the histogram as shown in Fig. 4, the iterative threshold method is used to obtain the threshold through the following four steps:

Step 1 Selecting an initial threshold T_0 which is better to be an average pixel gray of the image.

Step 2 Separately calculating the mean pixel grayscale levels of the parts separated by the iterative threshold T_k which is obtained from the last iteration. The kernel equation is given by

$$\begin{cases} \mu_1 = \sum\limits_{i=0}^{T_k} (h_i i) / \sum\limits_{i=0}^{T_k} h_i, \\ \mu_2 = \sum\limits_{i=T_k}^{255} (h_i i) / \sum\limits_{i=T_k}^{255} h_i, \end{cases} \tag{3}$$

where i is the pixel grayscale level ranging from 0 to 255, μ_1 and μ_2 are the mean pixel grayscale levels of the corresponding parts, respectively.

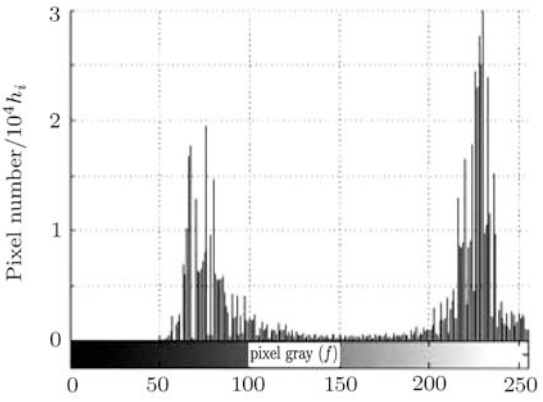


Fig. 4. Histogram of the sample.

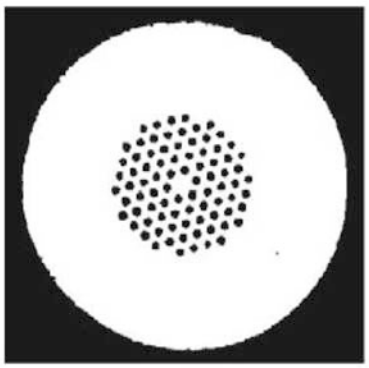


Fig. 5. Binary image of the sample.

Step 3 Calculating the new threshold value T_{k+1} defined by the following expression:

$$T_{k+1} = (\mu_1 + \mu_2)/2. \tag{4}$$

Step 4 Repeating Steps 2 and 3 until the threshold value T_k in successive iterations do not change. Thus the final threshold setup is obtained.

After the threshold is calculated, a binary image shown in Fig. 5 can be set up from the enlarged cross-section image of PCF in Fig. 2.

Sometimes, noises may be introduced by unclear fibre cross-section or image selecting device. Some noises can be eliminated by the binary processing, but

some cannot. For example, as shown in Fig. 6, the blotch will be enlarged with the image magnification increasing but still exist after the binary processing as shown in Figs. 7(a) and 7(b). In order to eliminate this type of noise, mathematical morphology, a technique of image processing based on shapes used to process binary for noise elimination and edge detection,[23] is employed. The method includes some fundamental morphological operations[24] such as the erosion, dilation, opening, closing, and so on. Opening and closing operations are often used in combination to eliminate noise and the result is shown in Fig. 7(c) where the blotch can be eliminated by this method.

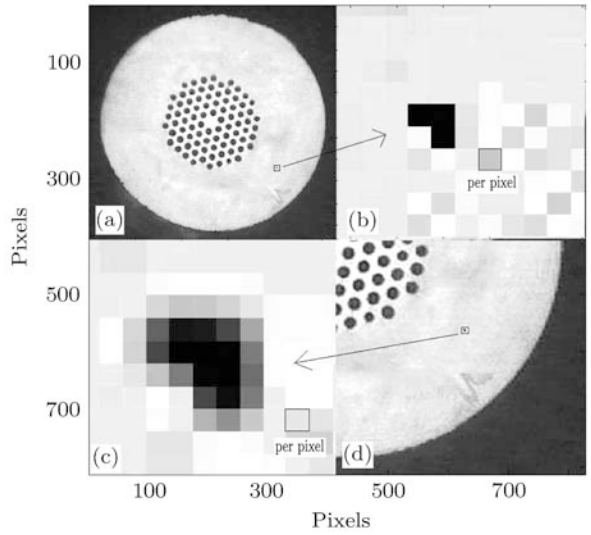


Fig. 6. Original cross-section image of our sample (a), noises on the original image (b), enlarged noise (c), and enlarged image (d).

Quite a lot of methods may be used in edge detection, they are the Laplace operator, Sobel operator, Gradient operator, etc. The mathematical morphology method can also be used in edge detection by the mathematical morphology edge detection operator which is defined as the original image subtracting the eroded image from the original by erosion operator. This method is better than others in the sense of edge continuity.[25] Using the mathematical morphology edge detection operator, the discrete edge in Fig. 8(a) can be extracted easily from the binary image. Figure 8(b) shows the rebuilt result obtained by the least square fitting method, which is used to deal with the discrete edges of each region, and the coordinate system transforms from the pixel coordinate system into a new coordinate system corresponding to the actual fibre size by using Eq. (5).

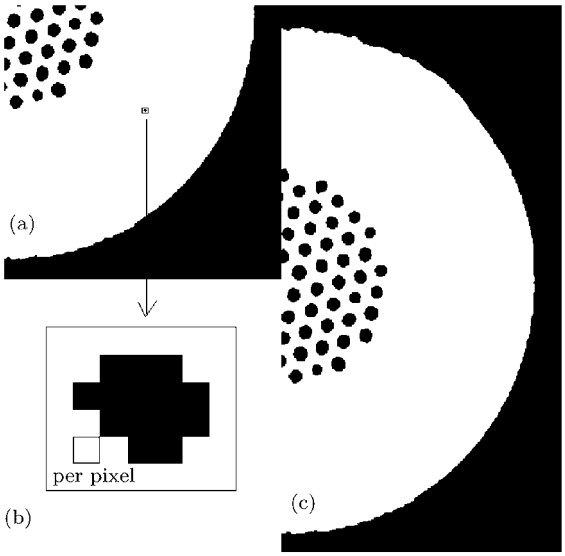


Fig. 7. (a) Binary image of the sample, (b) local amplification of the noise, and (c) binary image after noise eliminating.

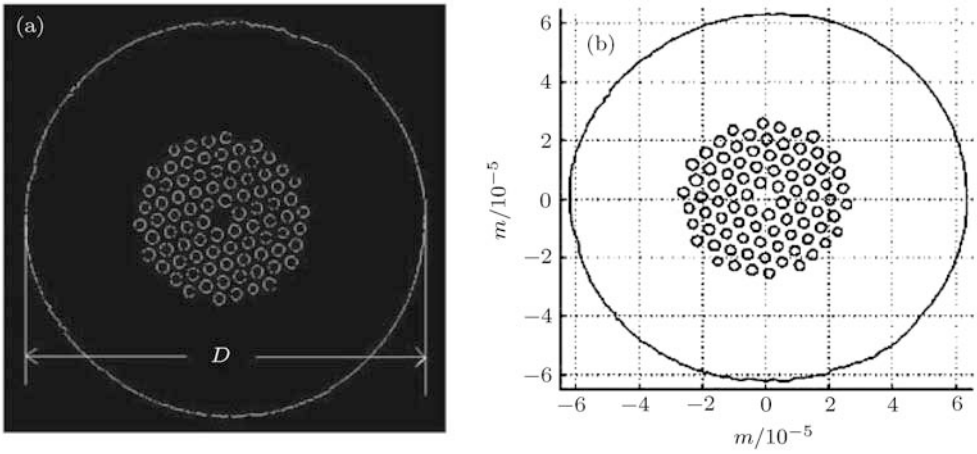


Fig. 8. (a) Binary edge and (b) rebuilt geometry of the sample.

$$\begin{cases} x_{\text{new}} = C\,(x_{\text{pixel}} - x_0), \\ y_{\text{new}} = C\,(y_{\text{pixel}} - y_0), \end{cases} \tag{5}$$

where the scaling coefficient C is denoted by the ratio of the outer diameter of the actual fibre to the pixel diameter that is defined as D, and the (x_0, y_0) are the position of central pixel of the geometry in the pixel coordinate system which can be obtained by averaging over the discrete edge pixels in the outer diameter of fibre.

2.2. Investigation on optical properties of actual PCF by finite element method

Finite element method is a powerful tool for modeling the properties of the fibre with an arbitrary geometry and has been widely used for analysing photonic crystal fibre due to its high accuracy and strong adaptability. Here, the finite element method with second order interpolation function[26] is employed for investigating the optical properties of the actual PCF with the rebuilt cross-sectional geometry.

As a key step, the mesh should be generated first. The rebuilt cross-sectional geometry is generated by using the triangle elements through the mesh generator in Matlab 7.0 and the generating process follows the mesh generating principle that the meshes in the central region and near the boundary are denser than those in other regions as shown in Fig. 9.

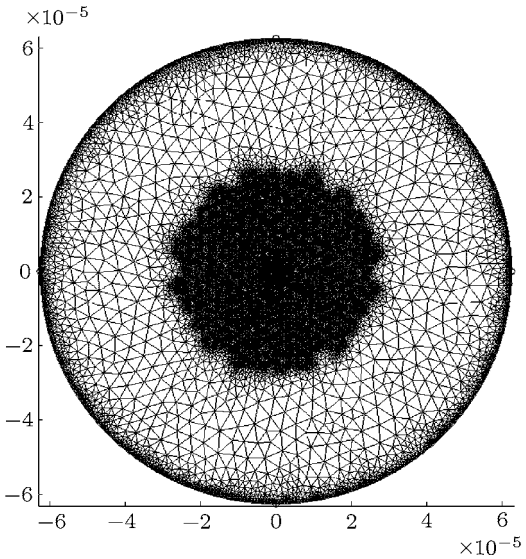


Fig. 9. Finite element meshes of the sample.

Then a full vectorial analysis of the electromagnetic field is achieved. From Maxwell's equations, the basic equation of the finite element method for obtaining the determination of the effective index of modes is given by

$$\boldsymbol{\nabla} \times \left(\varepsilon_{\text{r}}^{-1} \boldsymbol{\nabla} \times \boldsymbol{H}\right) - k_0^2 n_{\text{eff}}^2 \boldsymbol{H} = 0, \tag{6}$$

where $\boldsymbol{H}$ is the magnetic field, k_0 denotes the free-space wave number, ε_{r} is the relative dielectric permittivity, and n_{eff} is the effective index of modes. With the triangle element meshes, the eigenvalue equation (6) can be discretized and solved.

After obtaining the effective index n_{eff} and the magnetic H of modes, the other optical properties including the effective mode area, nonlinear coefficient, chromatic dispersion and beat length, can be calculated.[26]

In the following section, some optical properties of two kinds of photonic crystal fibres will be studied to verify the accuracy of this method.

3. Analysing optical properties of photonic crystal fibres

With this novel method, different types of photonic crystal fibres including a large mode area PCF and a polarization maintaining PCF made by the Crystal Fiber A/S are modeled.

3.1. Large mode area photonic crystal fibre

Figure 10 shows the cross section of a large mode area photonic crystal fibre made by the Crystal Fiber A/S, whose core diameter is 4.9 μm.[27] The holey region is extracted with the above method and meshed as shown in Fig. 11. The meshes are refined in the PCF core and the air–silica interfaces where there is quite a large refractive index step.

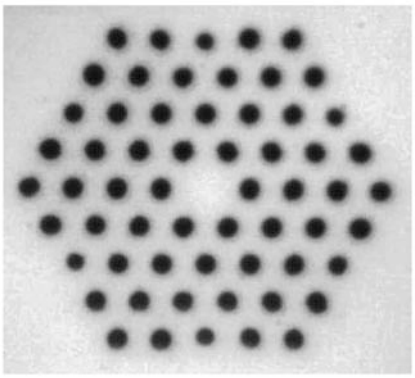


Fig. 10. Cross section of holey region of a large mode area photonic crystal fibre.

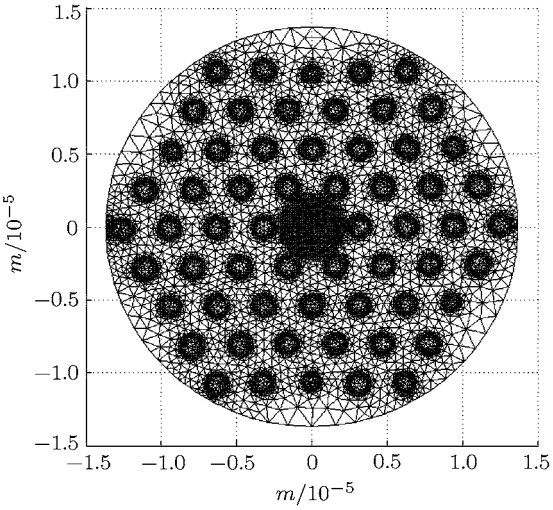


Fig. 11. Finite element meshes of the holey region.

After the edge extraction and geometry formation, some fibre parameters, such as the air holes diameter d and the hole-pitch Λ, can be obtained to be about 1.29 μm and 3.165 μm respectively, then the relative hole-size is $f = d/\Lambda = 0.4076 < 0.41$ from the rebuilt geometry of the fibre. After generating the finite element meshes, the properties of this fibre can be modeled with the finite element method in a wavelength range from 0.4 μm to 1 μm. Table 1 gives the numerical results obtained from our method and the given results by the Crystal Fiber A/S at the mode field diameters of the two orthogonal polarizations of the fundamental mode. The modal field area of the fundamental mode calculated by our method is accordant with the product data given by the Crystal Fiber A/S.

Table 1. Mode field diameter of the two orthogonal polarizations of the fundamental mode.

wavelength/μm	0.4	0.5	0.7	0.9	1.0
given results of mode field diameter/μm			4.2–0.5∼4.2+0.5		
numerical results of mode field diameter 1/μm	4.0682	4.0978	4.1605	4.2283	4.2645
numerical results of mode field diameter 2/μm	4.0665	4.0958	4.1575	4.2244	4.2601

3.2. Polarization maintaining photonic crystal fibre

As shown in Fig. 12, this PM–PCF has hole-pitch $\Lambda = 4.4$ μm, small hole diameter $d_1 = 2.2$ μm, large hole diameter $d_2 = 4.5$ μm, holey region diameter about 40 μm and outside diameter 125 μm.[28]

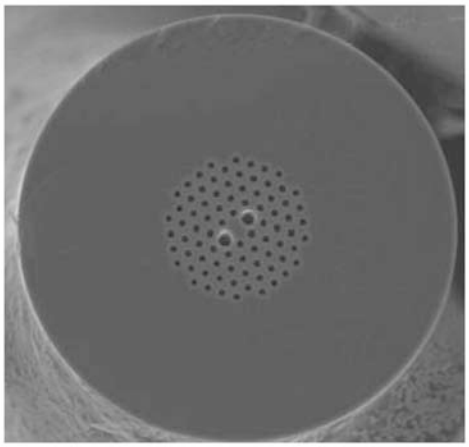


Fig. 12. Cross section of a polarization maintaining photonic crystal fibre.

Because the main influence on the properties lies in the structure of the inner air holes. In order to reduce the computer memory capacity needed and improve operation speed, we just calculate the inner four ring air-holes without loss of accuracy,[29,30] and the meshes are shown in Fig. 13. The dispersion and the beat length at wavelength 1550 nm are modeled and the numerical results by our method and the given results by the Crystal Fiber A/S are listed in Table 2. It is clear that those results are consistent with each other.

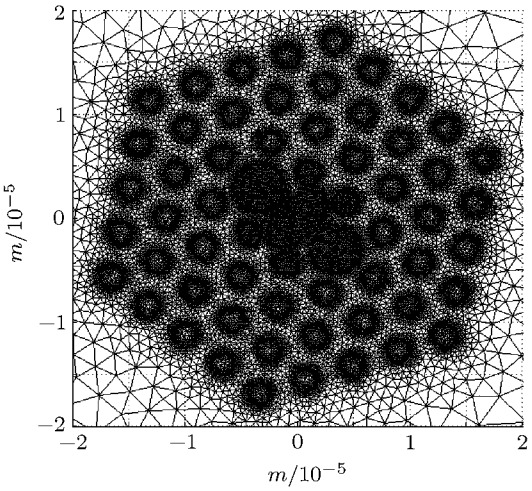


Fig. 13. Meshes of the inner four ring air-holes of the polarization maintaining PCF.

Table 2. Comparison of the numerical results with the product parameter.

$\lambda = 1550$ nm	dispersion of two polarizations		beat length/mm
given results	54	59	< 4
numerical results	54.5	58.8	3.33

The measuring process of the two PCFs described above has proved that when this tool runs on the computer with Intel P4 2.8 GHz and 2G RAM, the whole process consumes only about 3 min. This means that the method is fast and convenient enough to understand the optical properties of the actual fibre.

4. Conclusion

In order to quickly and conveniently understand the optical properties before use, a novel method is proposed for rapidly and accurately measuring the actual photonic crystal fibre in this paper. This method, which is based on the combination of digital image processing technique and finite element method, just requires a cross-sectional image of PCF, whose main part is completed by computer, so its operation is simple and convenient and the whole measuring period consumes a short time. Two kinds of PCFs made by Crystal Fiber A/S are modeled by this method and the comparison between the numerical results and the given results proves the accuracy of the proposed method. The features of this method imply that this method is suitable to the investigation of the properties of PCF for designing, simulating and optimizing the device or the system before the applications. In addition, this method can also be used to monitor the properties of the no-coated PCF for improving the PCF fabrication technology and providing required photonic crystal fibres for applications.

References

[1] Knight J C, Birks T A, Russell P S J and Atkin D M 1996 *Opt. Lett.* **21** 1547

[2] Liu X Y, Zhang F D, Zhang M and Ye P D 2007 *Chin. Phys.* **16** 1710

[3] Li Y Z, Qian L J, Lu D Q, Fan D Y and Chen G H 2008 *Chin. Phys.* B **17** 205

[4] Zhang X, Hu M L, Song Y J, Chai L and Wang Q Y 2010 *Acta Phys. Sin.* **59** 1863 (in Chinese)

[5] Palavicini C, Jaouen Y, Debarge G, Obaton A F, Kerrinckx E, Quiquempois Y, Douay M and Lepers C 2004 *Proceedings of IEEE of 17th Conference on Lasers and Electro-Optics Society* Washington, May 16–21, 2004, CWA67

[6] Liu X M, Wang Z F, Hou J, Jin A J and Liang D M 2009 *Asia Communications and Photonics Conference and Exhibition* Shanghai, November 2–6, 2009, WL35

[7] Cohen L G 1985 *J. Lightwave Technol.* **3** 958

[8] Hansen T P, Broeng J, Libori S E B, Knudsen E, Bjarklev A, Jensen J R and Simonsen H 2001 *IEEE Photon. Technol. Lett.* **13** 588

[9] Suzuki K, Kubota H, Kawanishi S, Tanaka M and Fujita M 2001 *Opt. Express* **9** 676

[10] Nielsen M D, Vienne G, Jensen J R and Bjarklev A 2002 *Proceedings of IEEE of 14th Conference on Lasers and Electro-Optics Society* San Diego, November 12–13, 2001, 707

[11] Genty G, Ludvigsen H, Kaviola M and Hansen K P 2004 *Opt. Express* **12** 929

[12] Ritari T, Niemi T, Ludvigsen H, Wegmuller M, Gisin N, Folkenberg J R and Petterson A 2003 *Opt. Commun.* **226** 233

[13] Folkenberg J R, Nielsen M D, Mortensen N A, Jakobsen C and Simonsen H R 2004 *Opt. Express* **12** 956

[14] Peyrilloux A, Chartier T, Hideur A, Berthelot L, Melin G, Lempereur S, Pagnoux D and Roy P 2003 *J. Lightwave Technol.* **21** 536

[15] Zhang Y N, Miao R C, Ren L Y, Wang H Y, Wang L L and Zhao W 2007 *Chin. Phys.* **16** 1719

[16] Lou S Q, Wang Z, Ren G B and Jian S S 2004 *Chin. Phys.* **13** 1493

[17] Folkenberg J R, Mortensen N A, Hansen K P, Hansen T P, Simonsen H R and Jakobsen C 2003 *Opt. Lett.* **28** 1882

[18] Tian H D, Yu Z Y, Han L H and Liu Y M 2009 *Chin. Phys.* B **18** 1109

[19] Meng J, Hou L T, Zhou G Y, Gao F, Yuan J H and Wei D B 2008 *Chin. Phys.* B **17** 3779

[20] Keys R G 1981 *IEEE Transactions on Acoustics, Speech, and Signal Processing* **29** 1153

[21] Hou H S and Andrews H C 1978 *IEEE Transactions on Acoustics, Speech, and Signal Processing* **26** 508

[22] Zhang A Z, Liu Z L, Zou X C and Xiang Z Q 2007 *Microelectronics & Computer* **24** 49 (in Chenese)

[23] Sartor L J and Weeks A R 2001 *J. Electronic Imaging* **10** 548

[24] Waheeb A U, Akram M and Ziad A A 2009 *European Journal of Scientific Research* **27** 167

[25] Zhang W W and Liu X F 2006 *Computer & Digital Engineering* **34** 59 (in Chinese)

[26] Poli F, Cucinotta A and Selleri S 2007 *Photonic Crystal Fiber—Properties and Application* (The Netherlands: Springer) pp. 219–223

[27] Crystal Fibre A/S http://www.crystal-fibre.com/datasheets/LMA-PM-5.pdf [2008]

[28] Crystal Fibre A/S http://www.crystal-fibre.com/datasheets/PM-1550-01.pdf [2008]

[29] Wang L W, Lou S Q, Chen W G and Fang H 2007 *Asia Optical Fibre Communication & Optoelectronic Exposition* Shanghai, Octtober 17–19, 2007 p. 370

[30] Steel M J, White T P, Sterke C M D, McPhedran R C and Botten L C 2001 *Opt. Lett.* **26** 488